THE JOURNAL OF PHYSICAL CHEMISTRY B

ARTICLE

pubs.acs.org/JPCB

Dissociation of Strong Acid Revisited: X-ray Photoelectron Spectroscopy and Molecular Dynamics Simulations of HNO_3 in Water

Tanza Lewis,[†] Bernd Winter,[‡] Abraham C. Stern,[†] Marcel D. Baer,[§] Christopher J. Mundy,[§] Douglas J. Tobias,[*,†] and John C. Hemminger[*,†]

[†]Department of Chemistry, University of California, Irvine, Irvine, California 92697, United States

[‡]Helmholtz-Zentrum Berlin für Materialien und Energie, and BESSY D-12489 Berlin, Germany

[§]Chemical and Materials Sciences Division, Pacific Northwest National Laboratory, Richland, Washington 99352, United States

ABSTRACT: Molecular-level insight into the dissociation of nitric acid in water is obtained from X-ray photoelectron spectroscopy and first-principles molecular dynamics (MD) simulations. Our combined studies reveal surprisingly abrupt changes in solvation configurations of undissociated nitric acid at approximately 4 M concentration. Experimentally, this is inferred from shifts of the N1s binding energy of $HNO_3(aq)$ as a function of concentration and is associated with variations in the local electronic structure of the nitrogen atom. It also shows up as a discontinuity in the degree of dissociation as a function of concentration, determined here from the N1s photoelectron signal intensity, which can be separately quantified for undissociated $HNO_3(aq)$ and dissociated $NO_3^-(aq)$. Intermolecular interactions within the nitric acid solution are discussed on the basis of MD simulations, which reveal that molecular HNO_3 interacts remarkably weakly with solvating water molecules at low concentration; around 4 M there is a turnover to a more structured solvation shell, accompanied by an increase in hydrogen bonding between HNO_3 and water. We suggest that the driving force behind the more structured solvent configuration of HNO_3 is the overlap of nitric acid solvent shells that sets in around 4 M concentration.

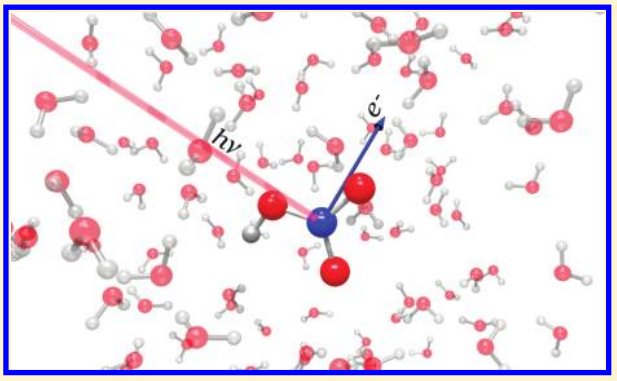

INTRODUCTION

Dissociation of strong acids in water is of enormous importance for a large class of chemical reactions in aqueous solutions.[1] Yet, our molecular-level understanding of this proton-transfer reaction for the simple case of nitric acid $HNO_3(aq) + H_2O(aq) \rightarrow H_3O^+(aq) + NO_3^-(aq)$ (reaction 1) is not complete. Even the experimental value of the degree of dissociation $\alpha = [NO_3^-]/([NO_3^-] + [HNO_3])$ is not very accurately known, despite attempts to determine it by various methods dating back to the 1950s[2−5] and 1960s.[6−8] Probably the most precise values are from 1964,[7] based on proton magnetic-resonance and Raman-spectroscopy measurements, but especially the midconcentration range around 3-5 M remains puzzling. This is where at the low concentration end there would be sufficiently many water molecules for optimal H_3O^+ and NO_3^- solvation, but as the concentration increases, solvation shells overlap. Changes in solvation of the reactant, molecular HNO_3, and the ionic products, NO_3^- and H_3O^+, contribute to determining the extent to which reaction 1 is favorable as the concentration is increased. In the present study we revisit the concentration dependence of the dissociation of nitric acid in water based on a combination of experiments and theoretical electronic-structure-based MD simulations.

Experimentally we use photoelectron (PE) spectroscopy from a vacuum liquid microjet in conjunction with soft X-ray synchrotron radiation to measure N1s photoelectrons from nitric acid aqueous solutions. The small size of the jet enables accurate detection of electron energies despite the high vapor pressure. In our experiments the excitation photon energy was adjusted to detect N1s photoelectrons from bulk nitric acid aqueous solution. The N1s binding energy is sensitive to even small changes in the chemical environment of the nitrogen atom. That is, the N1s PE contribution from $HNO_3(aq)$ and $NO_3^-(aq)$ can be distinguished, and the species can be quantified in terms of their relative concentrations. In addition, more subtle core-level energy shifts associated with changes in the solvation can be resolved. We detect such a shift in the local nitrogen environment of undissociated HNO_3 with concentration, and propose that it results from a change in the solvent configuration around $HNO_3(aq)$. We complement our experimental studies with first-principles molecular dynamics (FPMD) simulations that provide insight into the changes in the structure of the solution as the nitric acid concentration is increased.

FPMD simulations employing techniques similar to those used here, specifically, a density functional theory approach to the electronic structure with the BLYP exchange-correlation

Received: June 13, 2011
Revised: June 21, 2011
Published: June 21, 2011

functional, have been used previously to investigate HNO_3 in water.[9,10] The goals of the previous simulations, which consisted of a single HNO_3 molecule and 37[9] or 64[10] water molecules, were primarily to elucidate the mechanism of HNO_3 dissociation, and the difference between the dissociation in bulk water and near the air−water interface. Here our focus is on the changes (or lack thereof) in the solvation of the reactant and products, namely HNO_3, NO_3^-, and H_3O^+, that occur in bulk solution as the concentration is changed over a wide range (from 0.6 to 5 M). Because our simulations are relatively long compared to the previous work, we are able to develop a picture of the solvation in terms of distribution functions and hydrogen-bond statistics. Another difference between our simulations and the previous work is that we have included an empirical dispersion correction that alleviates some well-known deficiencies of the BLYP functional, which include a significant under-prediction of the density and concomitant overstructuring of liquid water at ambient conditions.[11−13]

The picture that emerges from our simulations is that HNO_3 interacts weakly with water at low concentration. At high concentration, the solution becomes crowded with solute, the solvation shells overlap, and the relative paucity of water promotes water−HNO_3 interactions. The signatures of crowding and solvent shell overlap appear at ∼4 M, which is where the experimental data hint at a change in the solvation of HNO_3. In contrast to molecular HNO_3, the solvation of the dissociation products, NO_3^- and H_3O^+, is essentially the same over the entire range of concentrations considered. We conclude, therefore, that the experimentally measured dependence of the extent of dissociation vs HNO_3 concentration can be understood based on the solvation of molecular HNO_3. We speculate that changes in solvation that occur with increasing concentration stabilize the molecular form and shift the dissociation equilibrium to the left (toward HNO_3).

METHODS

Experimental Section. Photoemission measurements were performed from a 15-μm sized liquid vacuum jet at the soft-X-ray U41 PGM undulator beamline of BESSY, Berlin.[14] The jet velocity was approximately 50 ms^{-1}, and the jet temperature was set at 4 °C, unless otherwise noted. Electrons were detected normal to both the synchrotron-light polarization vector and the flow of the liquid jet. A 100-μm diameter orifice that forms the entrance to the hemispherical electron energy-analyzer is at approximately 0.5 mm distance from the liquid jet, which is a short enough distance to ensure that detected electrons have not suffered from inelastic scattering with gas-phase water molecules around the small sized liquid jet. At operating conditions the pressure in the interaction chamber was about 1.5×10^{-4} mbar. The energy resolution of the U41 beamline is better than 300 meV at the incident photon energy of 1157 eV used here, and the resolution of the hemispherical energy analyzer is constant with kinetic energy (about 200 meV at 20 eV pass energy). For the current measurements of N1s spectra, 1157 eV photons produce photoelectrons of >750 eV kinetic energy, which corresponds to primarily probing the bulk solution, into a depth of approximately 50 Å.[15,16] The small focal size, 23×12 μm^2, of the incident photon beam allows for matching spatial overlap with the liquid microjet, reducing the gas-phase contributions of the measured spectra to less than 5%. The aqueous solutions were prepared from 70% HNO_3 in water (Sigma Aldrich), diluted in deionized water. Concentrations of 0.7−7.8 M were studied here.

Table 1. Compositions and dimensions of simulated systems

solution	no. of HNO_3 or NO_3^-	no. of water molecules	box length (Å)
0.6 M NO_3^-	1	96	14.400
0.6 M HNO_3	1	96	14.400
2 M HNO_3	3	82	13.773
3 M HNO_3	4	74	13.427
4 M HNO_3	6	83	14.094
5 M HNO_3	7	78	14.016

Computations. Simulations were carried out using the CP2K software suite (http://cp2k.berlios.de). The forces were computed via the QuickStep module, which contains an accurate and efficient implementation of density functional theory using dual basis sets of Gaussian type orbitals (TZV2P) and plane waves (expanded to Ecut =280 Ry) for the electron density.[17] Only the valence electrons were considered explicitly, and the core−electron states were represented via Goedecker-Teter-Hutter pseudopotentials.[18] The Grimme dispersion correction was used in conjunction with the Becke exchange and Lee−Yang−Parr correlation (BLYP) functional.[19−21] It has been demonstrated that the BLYP/TZV2P theoretical model provides a reasonable description of the effects of solvation on proton transfer.[11] The dispersion correction has recently been shown to vastly improve the density and structure of the BLYP description of water at near ambient conditions.[12,13] We expect that dispersion corrections will also improve the BLYP description of nitric acid−water interactions, but this has yet to be demonstrated.

In total, six systems were simulated using FPMD. Solutions of nitric acid were prepared at concentrations 2, 3, 4, and 5 M. In addition, we simulated two relatively dilute (∼0.6 M) model systems. One system consisted of a single, water-solvated HNO_3(aq) molecule in which the O−H bond was restrained to prevent dissociation, and hence serves as an idealized model of the protonated state. The second system was a single, solvated NO_3^-(aq) ion with a charge compensating background that serves as an idealized model of the unprotonated state. Details of the system sizes and compositions are provided in Table 1. All systems were simulated for approximately 25 ps.

All of the systems were contained in cubic boxes with periodic boundary conditions applied in three dimensions. The simulations were performed in the canonical ensemble at 300 K by coupling Nose-Hoover chain thermostats to every degree of freedom.[22] The classical equations of motion for the nuclei were evolved using Born-Oppenheimer dynamics with a time step of 0.5 fs and a wave function minimization tolerance of 10^{-6} H.

RESULTS AND DISCUSSION

Figure 1 shows N1s PE spectra from bulk aqueous solution of nitric acid for 0.7, 2.5, and 7.8 M concentration. For comparison we also present the N1s PE spectrum from 1.5 M $NaNO_3$ aqueous solution (top tier), where NO_3^- is the only nitrogen-containing species. All spectra were acquired at 1157 eV photon energy. Electron energies are with respect to vacuum and were calibrated by the oxygen 1s binding energy (BE) of water.[23] Measurements from the 0.7 M nitric acid solution and from the

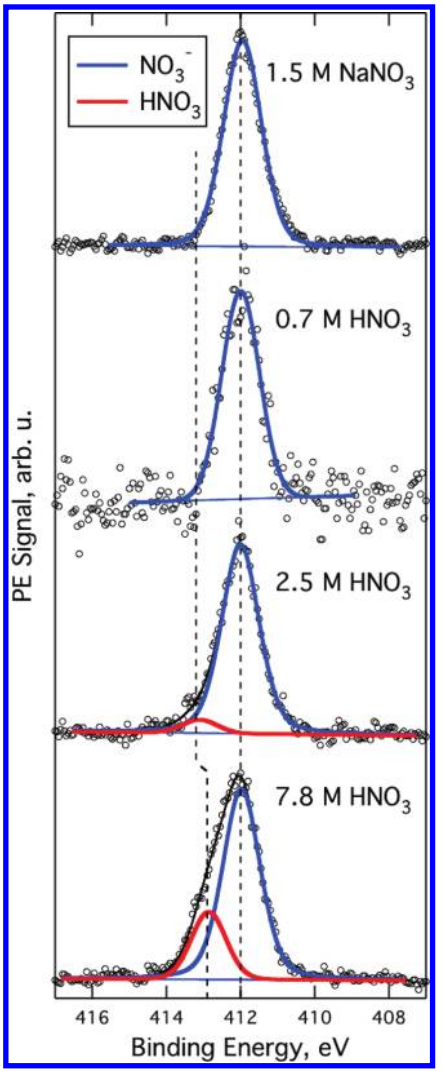

Figure 1. N1s photoelectron spectra of sodium nitrate and nitric acid aqueous solution measured at different bulk concentrations. Spectra were taken at 1157 eV photon energy. The two Gaussians used to fit the 2.5 and 7.8 M HNO_3 spectra represent signal from molecular HNO_3 and from NO_3^-, respectively. The binding energy of NO_3^- is 412.0 eV, whereas we observe binding energy shifts in molecular HNO_3 due to variation in solvation environment.

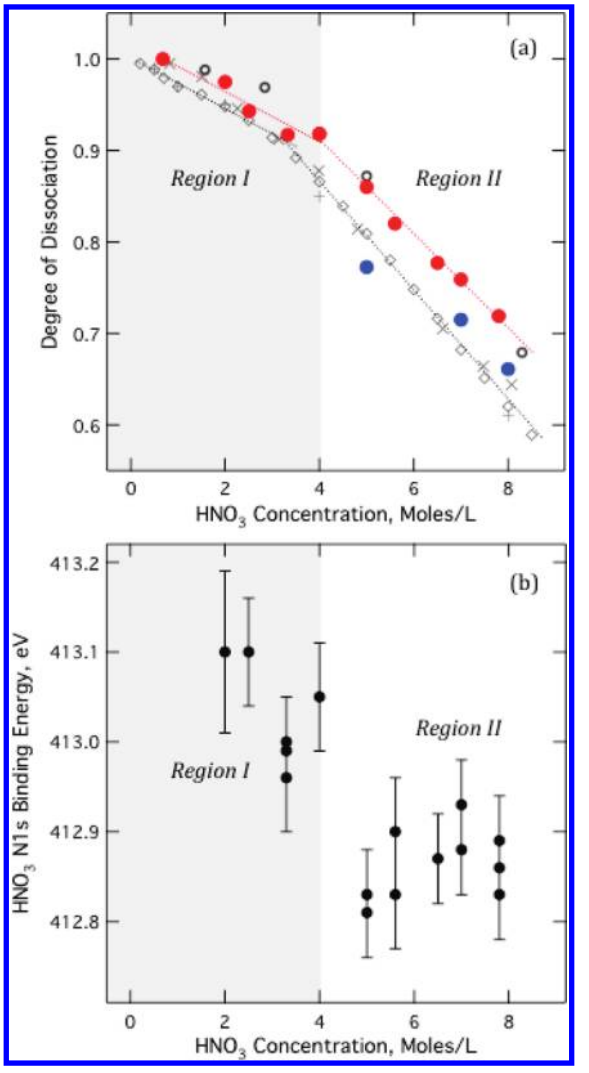

Figure 2. (a) Degree of HNO_3 dissociation in bulk solutions (α) as a function of nitric acid bulk concentration (This work: 4 °C red circles, 25 °C blue circles). Literature values of α are shown for comparison (diamonds;[7] crosses;[24] 25 °C, ×'s;[3] 0 °C, open gray circles[3]). We denote two regions, region I and II, separated by a discontinuity in dissociation that occurs near 4 M nitric acid concentration. (b) N1s binding energy of HNO_3 as a function of nitric acid concentration.

sodium nitrate solution yield N1s peaks at the same binding energy (412.0 eV) and same Gaussian peak width (1.9 eV), which would imply 100% dissociation ($\alpha = 1$) of HNO_3 in water at 0.7 M concentration. Note that an earlier reported value is $\alpha = 0.98$,[3] but the difference between this and $\alpha = 1.0$ is below our current experimental detection limit. The N1s spectrum measured at 2.5 M is asymmetric on the high-binding energy side. The asymmetry is due to a second N1s peak arising from undissociated HNO_3(aq). This contribution can be fit by a second Gaussian with peak maximum at 413.1 eV. The signal due to molecular HNO_3(aq) continues to grow with increasing concentration as dissociation becomes less probable. The observed higher BE of the neutral form results from the lower electron density at the nitrogen site in HNO_3(aq) compared to NO_3^-(aq). With increasing concentration the BE of HNO_3 is found to decrease slightly. For instance, the energy shift between HNO_3(aq) and NO_3^-(aq) for 2.5 M concentration is 0.2 eV larger than for 7.8 M. We will see below that this shift is not linear over the concentration range investigated. Since the kinetic energies of the emitted photoelectrons are essentially identical for the molecular and dissociated species (and so are the respective probing depths into the bulk solution), the cross sections for N1s core ionization are expected to be the same, and the nitrogen 1s PE intensity ratios of Figure 1 are therefore a direct and very accurate measure of the relative concentrations of the two molecular forms. Thus, for each concentration we can precisely determine the experimental value of α, within the limits of signal-to-noise.

Values of α obtained from PE spectra measured at several concentrations are plotted in Figure 2a (red full circles). Experimental error corresponds to the circle size, and primarily originates from small uncertainties in solution concentration as well as from the small HNO_3 signal-to-noise ratio at the lower concentrations. We find that the slope of α vs concentration

dx.doi.org/10.1021/jp205510q |J. Phys. Chem. B 2011, 115, 9445–9451

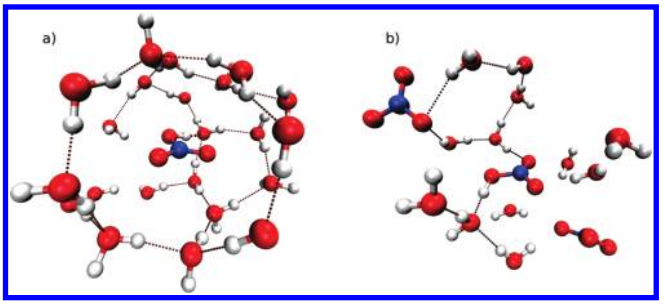

Figure 3. Representative snapshots from FPMD simulations of HNO_3 at (a) low concentration (0.6 M), and (b) high concentration (5 M), where other nitrate species are present in the first solvation shell.

changes at ~4 M. The dependence of α on $[HNO_3]$ is linear above 4 M, but whether the change in the <4 M region is also strictly linear cannot be answered from our data. However, comparison with previous works[3,7,24] would suggest that at ~4 M there is indeed a reproducible turnover from smaller to larger slope. This is particularly evident from the set of measurements published by Davis in 1963, and others, all shown in Figure 2a along with the present PE data. Curiously, though, none of the previous reports has mentioned the apparent turnover in α vs $[HNO_3]$. Note that the slightly larger values of α in the current work are due to the lower temperature (4 °C) of the solution for our measurements. This is confirmed by a few single-point PE measurements at 25 °C, and is also consistent with the 0 °C data of Krawetz[3] (see Figure 2).

The occurrence of two distinct regions of α, which we denote I and II, separated at approximately 4 M nitric acid concentration implies some qualitative change in the details of the dissociation conditions, the explanation of which requires information on the interactions between HNO_3, NO_3^-, H_3O^+ and the surrounding water molecules that is not available from the experimental results in Figure 2a alone. To gain additional insight we have (i) analyzed the N1s binding energy shifts of HNO_3(aq) as a function of concentration, and (ii) performed FPMD simulations to advance our understanding of microscopic details of the accommodation of HNO_3, NO_3^-, and H_3O^+ in water, again as a function of concentration. Figure 2b shows the experimental N 1s BEs of HNO_3(aq) as a function of concentration. While the observed energy shifts are small (not larger than 300 meV), and the data are scattered due to limitations in signal-to-noise for low HNO_3 concentrations, we observe a clear correlation with the change of slope in the plot of α versus concentration that occurs near 4 M concentration: the HNO_3(aq) binding energy is higher for low solution concentrations and decreases discontinuously at ~4 M. Throughout the low concentration range of region I (below 4 M) HNO_3(aq) has a BE between 413.0 and 413.1 eV. In contrast, throughout region II (above 4 M) the binding energy of HNO_3(aq) is constant at a value below 412.9 eV. Although it is difficult to connect BE changes with specific solvation configurations or mechanistic details in dissociation, the shift in BE provides strong support for our two-regime description of the dissociation behavior, and points to solvation-structure changes that occur in the nitric acid solution at ~4 M. We note that while we observe a shift in the N1s BE of HNO_3(aq), the BE of NO_3^-(aq) remains constant throughout the entire concentration range considered here. This suggests that the important changes relevant to the turnover point in α occur with HNO_3(aq), but not NO_3^-(aq) or H_3O^+(aq).

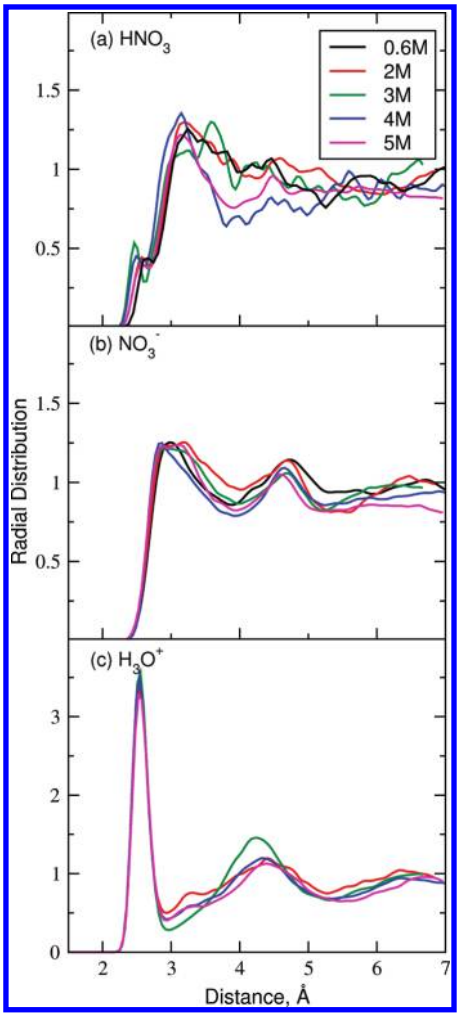

Figure 4. Radial distribution functions of water oxygen atoms around oxygens of (a) HNO_3, (b) NO_3^-, and (c) H_3O^+ shown at a series of nitric acid concentrations.

Now we turn to an exploration of the concentration-dependent changes in the solvation structure of both the products and reactants of reaction (1) using first-principles molecular dynamics simulations. To set the stage for the more detailed analysis that follows, we begin by looking at snapshots from the simulations of the two extremes of the concentration range. Figure 3a is a representative snapshot of undissociated HNO_3 at low concentration (~0.6 M). Water organizes around HNO_3 as if the molecule were hydrophobic, forming an ordered cage with extensive water−water hydrogen-bonding that is reminiscent of a clathrate-like structure; only one hydrogen-bond is formed with the acidic proton of HNO_3 acting as an H-bond donor and a water molecule as the acceptor. Such a structure is expected to be energetically less favorable, at least insofar as solvation is concerned, than the two ionic dissociation products NO_3^- and H_3O^+, which interact strongly with water via H-bonds (see below). Figure 3b is a representative snapshot of HNO_3 at high concentration (5 M). Here, in addition to an H-bond formed by the acidic proton, molecular HNO_3 forms one additional hydrogen bond with one of the unprotonated oxygen atoms acting as the acceptor and water as the donor. We see fewer water molecules around HNO_3 due to crowding from other nitric acid/nitrate molecules, and it appears that the water molecules

dx.doi.org/10.1021/jp205510q |J. Phys. Chem. B 2011, 115, 9445–9451

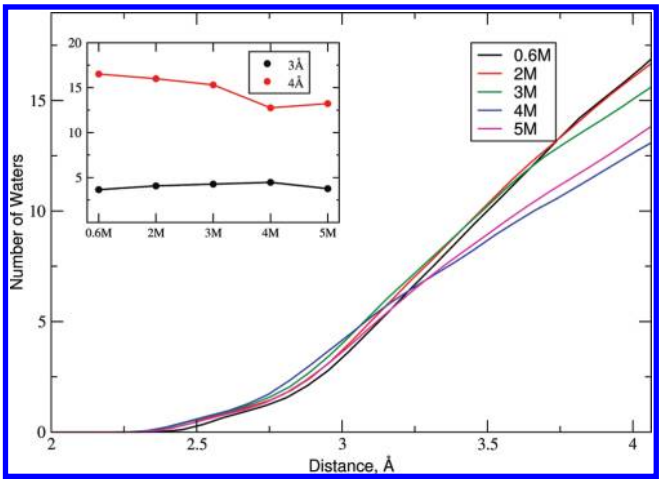

Figure 5. Coordination number of HNO_3 as a function of molecular radius shown for different nitric acid concentrations. Inset shows the number of water molecules within 3 Å (in black) and within 4 Å (in red) of HNO_3 as a function of concentration. With increasing concentration, the number of water molecules within a 4 Å shell decreases but increases slightly within a 3 Å shell.

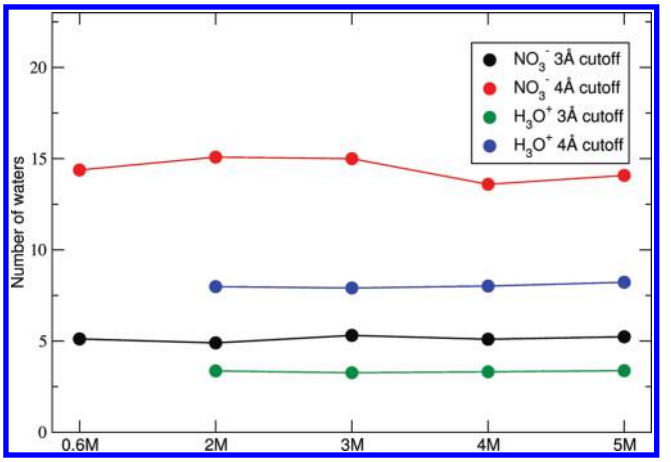

Figure 6. Number of water molecules around NO_3^- and H_3O^+ within a 3 and 4 Å molecular radius, shown as a function of nitric acid concentration. We observe essentially no change in the coordination number with concentration for both species.

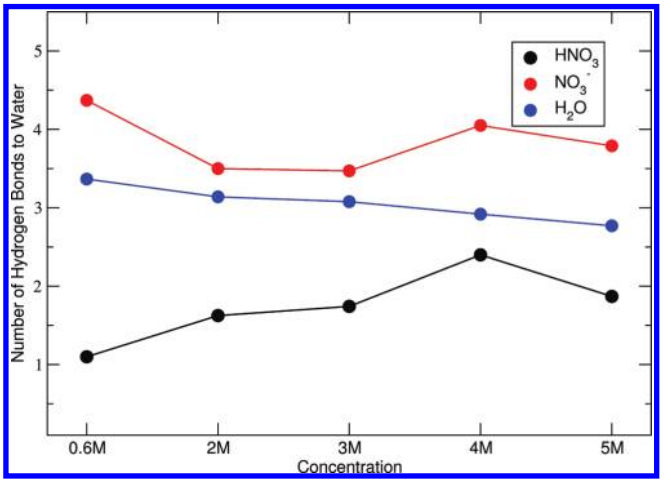

Figure 7. Number of water−NO_3^-, water−HNO_3, and water−water hydrogen bonds as a function of nitric acid concentration. NO_3^- accepts approximately four hydrogen bonds throughout the concentration range, whereas HNO_3 has only one hydrogen bond (corresponding to the donation of the proton to an acceptor water) at low concentration and accepts an additional hydrogen bond at high concentrations. Water−water H bonds are disrupted as the solute concentration increases.

that are present are less able to form hydrogen-bonds with each other and are rather forced to interact more strongly with HNO_3.

Solvation shell structure is conveniently discussed in terms of radial distribution functions (RDFs). The RDFs of water around the oxygens of HNO_3, shown in Figure 4a, exhibit several noteworthy features. At low concentrations (0.6 to 3 M), the RDFs are quite similar and they do not display a clear minimum beyond the first peak, whereas at 4 and 5 M there is a clear minimum at $r \sim 4$ Å that indicates a more well-defined solvation shell. Note that the change in solvation of HNO_3 that occurs at ~4 M concentration coincides with the experimentally observed BE shift and the change in slope of α vs $[HNO_3]$ (Figure 2). Also apparent in the RDFs in Figure 4a is the presence of a small peak at around 2.5 Å, corresponding to one water molecule interacting with the proton of HNO_3 (shown in the snapshot in Figure 3a). Figure 4, panels b and c, shows radial distribution functions for water around the oxygen atoms of the products of HNO_3 dissociation, NO_3^- and H_3O^+. Unlike the case of HNO_3, both sets of RDFs are relatively well structured throughout the entire range of concentrations, which is indicative of relatively tight first solvation shells. The fact that the RDFs of H_3O^+ and NO_3^- show essentially no concentration dependence (in contrast to those of HNO_3) is a strong indication that the experimentally observed changes in the BE and the slope of α vs concentration is primarily connected with changes in the solvation of HNO_3, but not H_3O^+ and NO_3^-.

To quantify hydration, we need a definition of the solvation shell. The criterion used here is the number of water oxygen atoms within a given distance of any heavy atom (N or O) in HNO_3. The dependence of this quantity on distance is shown for a series of nitric acid concentrations in Figure 5. The inset of Figure 5 shows the number of water molecules within 3 and 4 Å of HNO_3, respectively, as a function of concentration. We note two interesting features. First, the number of water molecules within 4 Å decreases with increasing concentration. At high HNO_3 concentrations, displacement of water by other nitrate species explains the loss of water within 4 Å. However, the number of water molecules within 3 Å is practically constant, and appears to increase slightly with concentration. The retention (and possible increase) in the number of water molecules within 3 Å and loss of water within 4 Å (Figure 5) is consistent with the sharpening of the first peak in the RDFs (Figure 4a) and reflects the tendency of water to interact more strongly with HNO_3, as the concentration increases. This shift to a tighter, more defined solvation shell is not observed in the RDFs of NO_3^- and H_3O^+ (Figure 4, panels b and c). The numbers of solvating water molecules within 3 and 4 Å of heavy atoms in NO_3^- and H_3O^+, plotted in Figure 6, remain constant for both species as a function of concentration, further corroborating the hypothesis that the experimentally observed changes of the slope of α versus concentration and the BE with concentration are primarily a manifestation of changes in the solvation of molecular HNO_3.

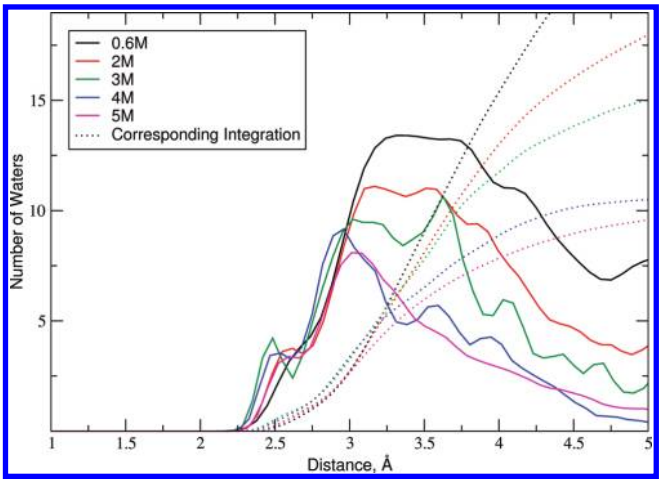

Figure 8. Distribution of distances from water to the nearest undissociated HNO_3 at a series of nitric acid concentrations. Dashed lines are the corresponding integrals of each trace. The loss in intensity between approximately 3 and 4 Å for higher concentrations corresponds with an onset of sharing of water molecules between HNO_3 and another nitrate species (HNO_3 or NO_3^-).

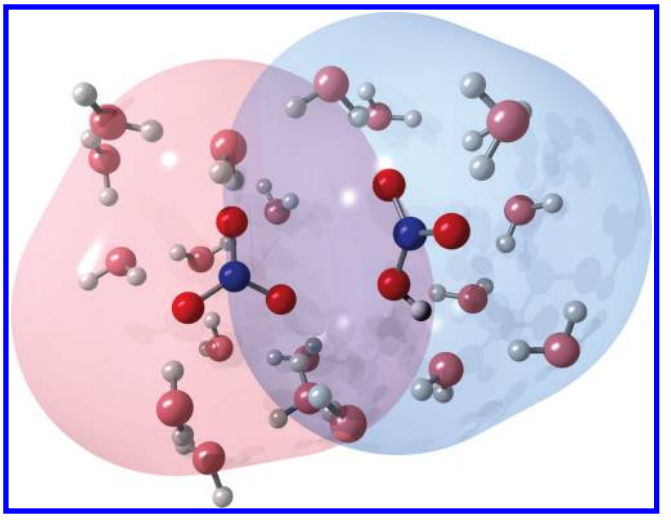

Figure 9. Representative snapshot depicting solvent shell overlap of HNO_3 and NO_3^- at high concentration. The solvation shell of HNO_3 is enclosed by the blue surface and that of NO_3^- by the red surface.

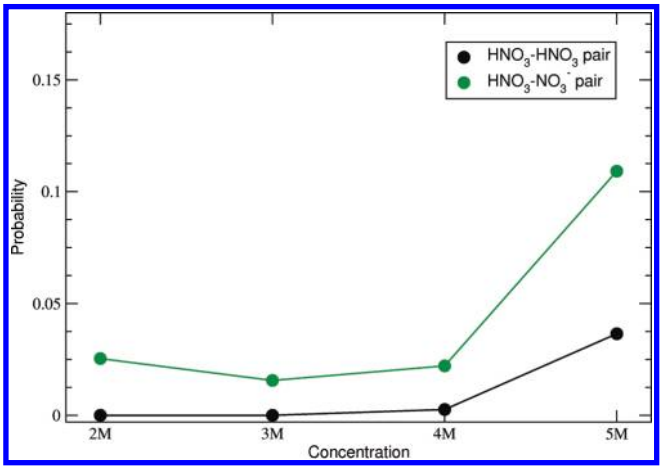

Figure 10. Probability of HNO_3–HNO_3 and HNO_3–NO_3^- pairs as a function of nitric acid concentration. The probability that HNO_3–NO_3^- pairs occur increases dramatically at 5M.

Now that we have quantified the amount of water present around HNO_3(aq) and its dissociation products, we quantify the degree of HNO_3–water and water–water hydrogen-bonding using standard criteria. We consider a hydrogen bond to exist if the distance between heavy atoms is less than 3.5 Å and O–H–O angle is greater than 150°. Figure 7 plots the number of H-bonds between water and HNO_3 or NO_3^- as a function of concentration. The number of H-bonds to the NO_3^- oscillates around four over the concentration range, consistent with the aforementioned tight first-solvation shell evidenced by the respective RDFs of Figure 4. In contrast, hydrogen bonding to HNO_3(aq) is scarce. At low concentrations HNO_3(aq) donates only one hydrogen bond—the HNO_3 proton to water oxygen—and accepts none. However, as the concentration increases, HNO_3(aq) gradually accepts an additional hydrogen bond, typically formed to an unprotonated oxygen rather than to the nitrogen or the protonated oxygen (see Figure 3 for representative snapshots). The additional HNO_3–water hydrogen bond comes at the expense of a water–water hydrogen bond at high HNO_3 concentration.

Taken together, the results of the solvation and hydrogen-bonding analyses presented so far suggest that, at high concentration, although we see an overall decrease in the number of water molecules within 4 Å of HNO_3, the water molecules that remain present within 3 Å are forced to interact more strongly (via H-bonds) with the apparently "hydrophobic" molecular HNO_3 species. Evidently, at high concentrations water is relatively scarce, and the lack of water–water H-bonding possibilities promotes the formation of an additional H-bond between water and HNO_3(aq). We note that our observation of the formation of HNO_3–water H-bonds only at high concentration differs from previous simulation studies that found HNO_3–water H-bonding at low concentration.[9,25] However, we note that previous simulations were conducted at different temperatures, namely 0 K[25] and ~240 K,[9] which may partially explain the discrepancy with our results.

Next we investigate the role of solute crowding in promoting the formation of hydrogen bonds to HNO_3 by analyzing the extent of sharing of solvent shells between HNO_3 and other nitrate species at high concentrations.To evaluate the degree to which the solvation shell of molecular HNO_3 is affected by the presence of neighboring nitrate species, we calculate the distribution of distances from water to heavy atoms in the nearest nitrate species. This measure will be sensitive to the extent that solvent shells overlap since water molecules between two NO_3 moieties will be binned according to whichever nitrate species is nearest. Histograms of the distances for a series of concentrations are shown in Figure 8; the running integrals of the histograms, shown as dashed lines, denote the number of water molecules within a particular distance of an HNO_3 molecule that are not closer to another nitrate species. We make several important observations concerning these data. First, as the concentration increases, the main peak in the water distributions shrinks, sharpens, and shifts to smaller distances. The loss of intensity near 3.5–4 Å is the result of water molecules moving into the solvent shells of other nitric acid or nitrate molecules. Note that the decrease in unshared water around HNO_3 occurs most

dx.doi.org/10.1021/jp205510q |J. Phys. Chem. B 2011, 115, 9445–9451

dramatically at 4 M nitric acid concentration, again consistent with the concentration at which we observe the experimental BE shift and the discontinuity in α as a function of concentration. A representative MD snapshot of HNO_3/NO_3^- solvent shell overlap at 5 M is shown in Figure 9, and the concentration dependence of the probability of finding such pairs, as well as HNO_3/HNO_3 pairs is shown in Figure 10. Here, pairing is considered to occur if any heavy atom of HNO_3 is within 3 Å of any heavy atom of another nitrate species (HNO_3 or NO_3^-). We observe that the overall probability of pairing grows with increasing concentration. However, HNO_3/NO_3^- pairs are essentially not observed until the HNO_3 concentration exceeds 4 M, at which point there is a dramatic increase in their probability to exist in solution. We speculate that pairing of this type (see Figure 9) contributes to the decrease in dissociation and the decrease in the N1s BE at high HNO_3 concentration (>4 M).

CONCLUSIONS

Dissociation of nitric acid in water was revisited on the molecular level, and it is found that several quantities defining the solvation structure of HNO_3(aq) change rather abruptly near 4 M concentration. Experimentally we observe a sudden decrease of nitrogen 1s electron binding energies of the undissociated acid when going from low to high concentrations at ∼4 M, as well as an increase in the slope of degree of dissociation that occurs within the same small concentration interval. First-principles MD simulations correlate these changes with a tighter solvation shell around HNO_3 for concentrations larger than 4 M due to more favorable hydrogen bonding with surrounding water molecules, which is a consequence of solute crowding and overlap of solvation shells. Despite the striking correlations between electronic energies and solvation structure we are currently unable to fully explain the origin of the sharp break in experimentally observed quantities. However, it is clear from our simulations that the lack of favorable hydrogen bonding between waters and HNO_3 contributes to the destabilization of the molecular form at low concentration. The unexpected "hydrophobic" solvation of molecular HNO_3 exposed here is also likely to be relevant to understanding the difference in the dissociation of HNO_3 at the solution surface vs in bulk solution.[9,10,25−27]

ACKNOWLEDGMENT

AirUCI under Grant CHE 0431312 from the NSF supported this work. Additional support from the Deutsche Forschungsgemeinschaft (Project WI 1327/3-1) is gratefully acknowledged. The work at Pacific Northwest National Laboratory (PNNL) was performed under the auspices of the Division of Chemical Sciences, Geosciences, and Biosciences, Office of Basic Energy Sciences, U.S. Department of Energy, under Contract No. DE-AC06-76RLO 1830 with Battelle Memorial Institute, which operates PNNL. The molecular dynamics simulations utilized the BlueGene/P at Argonne National Laboratory (resources of the Argonne Leadership Computing Facility at Argonne National Laboratory, which is supported by the Office of Science of the U.S. DOE under Contract No. DE-AC02-06CH11357) under an INCITE 2007-2010 award as well as computational resources from the National Energy Research Supercomputing Center (NERSC) at Lawrence Berkeley National Laboratory, the Molecular Sciences Computing Facility at PNNL, and the University of California Shared Research Computing Services (ShaRCS) pilot project. M.D.B. is grateful for the support of the Linus Pauling Distinguished Postdoctoral Fellowship program at PNNL. Manfred Faubel is gratefully acknowledged for help with the experimental technology and broad ranging discussions.

REFERENCES

(1) Atkins, P.; Jones, L. *Chemical Principles: the Quest for Insight*, 5th ed.; Freeman, W. H. and Co.: New York, 2010.
(2) Hood, G. C.; Redlich, O.; Reilly, C. A. *J. Chem. Phys.* **1954**, *22*, 2067.
(3) (a) Krawetz, A. A., The University of Chicago, 1955. (b) Young, T. F.; Maranville, L. F.; Smith, H. M. Raman Spectra Investigations of Ionic Equilibria in Solutions of Strong Electrolytes. In *The Structure of Electrolytic Solutions*; Hamer, W. J., Ed.; Wiley: New York, 1959; pp 35−63.
(4) McKay, H. A. C. *Trans. Faraday Soc.* **1956**, *52*, 1568.
(5) Redlich, O.; Hood, G. C. *Discuss. Faraday Soc.* **1957**, 87.
(6) Högfeldt, E. *Acta Chem. Scand.* **1963**, *17*, 785.
(7) Davis, W.; Debruin, H. J. *J. Inorg. Nucl. Chem.* **1964**, *26*, 1069.
(8) Redlich, O.; Duerst, R. W.; Merbach, A. *J. Chem. Phys.* **1968**, *49*, 2986.
(9) Wang, S. Z.; Bianco, R.; Hynes, J. T. *J. Phys. Chem. A* **2009**, *113*, 1295.
(10) Shamay, E. S.; Buch, V.; Parrinello, M.; Richmond, G. L. *J. Am. Chem. Soc.* **2007**, *129*, 12910.
(11) Mundy, C. J.; Kuo, I. F. W.; Tuckerman, M. E.; Lee, H. S.; Tobias, D. J. *Chem. Phys. Lett.* **2009**, *481*, 2.
(12) Schmidt, J.; VandeVondele, J.; Kuo, I. F. W.; Sebastiani, D.; Siepmann, J. I.; Hutter, J.; Mundy, C. J. *J. Phys. Chem. B* **2009**, *113*, 11959.
(13) Kühne, T. D.; Pascal, T. A.; Kaxiras, E.; Jung, Y. *J. Phys. Chem. Lett.* **2011**, *2*, 105.
(14) Winter, B. *Nucl. Instrum. Meth. A* **2009**, *601*, 139.
(15) Brown, M. A.; Winter, B.; Faubel, M.; Hemminger, J. C. *J. Am. Chem. Soc.* **2009**, *131*, 8354.
(16) Ottosson, N.; Faubel, M.; Bradforth, S. E.; Jungwirth, P.; Winter, B. *J. Electron Spectrosc. Relat. Phenom.* **2010**, *177*, 60.
(17) VandeVondele, J.; Krack, M.; Mohamed, F.; Parrinello, M.; Chassaing, T.; Hutter, J. *Comput. Phys. Commun.* **2005**, *167*, 103.
(18) Goedecker, S.; Teter, M.; Hutter, J. *Phys. Rev. B* **1996**, *54*, 1703.
(19) Grimme, S. *J. Comput. Chem.* **2006**, *27*, 1787.
(20) Becke, A. D. *Phys. Rev. A* **1988**, *38*, 3098.
(21) Lee, C. T.; Yang, W. T.; Parr, R. G. *Phys. Rev. B* **1988**, *37*, 785.
(22) Martyna, G. J.; Klein, M. L.; Tuckerman, M. *J. Chem. Phys.* **1992**, *97*, 2635.
(23) Winter, B.; Aziz, E. F.; Hergenhahn, U.; Faubel, M.; Hertel, I. V. *J. Chem. Phys.* **2007**, *126*, 124504.
(24) Querry, M. R.; Tyler, I. L. *J. Chem. Phys.* **1980**, *72*, 2495.
(25) Bianco, R.; Wang, S. Z.; Hynes, J. T. *J. Phys. Chem. A* **2007**, *111*, 11033.
(26) Schnitzer, C.; Baldelli, S.; Campbell, D. J.; Shultz, M. J. *J. Phys. Chem. A* **1999**, *103*, 6383.
(27) Soule, M. C. K.; Blower, P. G.; Richmond, G. L. *J. Phys. Chem. A* **2007**, *111*, 3349.